# Qutrit circuits and algebraic relations: A pathway to efficient spin-1 Hamiltonian simulation

Oluwadara Ogunkoya [1,*] Joonho Kim [2] Bo Peng [3,†] A. Barış Özgüler [1,‡] and Yuri Alexeev [4]

[1]*Superconducting Quantum Materials and Systems Center (SQMS), Fermi National Accelerator Laboratory, Batavia, Illinois 60510, USA*
[2]*Rigetti Computing, Berkeley, California 94710, USA*
[3]*Physical and Computational Sciences Division, Pacific Northwest National Laboratory, Richland, Washington 99352, USA*
[4]*Computational Science Division, Argonne National Laboratory, Lemont, Illinois 60439, USA*

Quantum information processing has witnessed significant advancements through the application of qubit-based techniques within universal gate sets. Recently, exploration beyond the qubit paradigm to $d$-dimensional quantum units or qudits has opened new avenues for improving computational efficiency. This paper delves into the qudit-based approach, particularly addressing the challenges presented in the high-fidelity implementation of qudit-based circuits due to increased complexity. As an innovative approach towards enhancing qudit circuit fidelity, we explore algebraic relations, such as the Yang-Baxter-like turnover equation, which may enable circuit compression and optimization. The paper introduces the turnover relation for the three-qutrit time propagator and its potential use in reducing circuit depth. We further investigate whether this relation can be generalized for higher-dimensional quantum circuits, including a focused study on the one-dimensional spin-1 Heisenberg model. Our paper outlines both rigorous and numerically efficient approaches to potentially achieve this generalization, providing a foundation for further explorations in the field of qudit-based quantum computing.

## I. INTRODUCTION

Quantum information processing through a gate-based quantum computing approach with qubits involves a universal gate set consisting of single-qubit gates in the SU(2) group and entangling two-qubit gates [1]. This approach has been intensively studied in recent years for applications in quantum information science. Particularly in the quantum error correction, the qubit-based surface code [2,3] has been thus far the primary route for error detection and correction [4–7].

Nevertheless, for certain specific applications, it has been discussed that a more generalized $d$-dimensional ($d > 2$) quantum unit, or qudit, might offer advantages over the qubit system. This is because the qudit-based approach allows exploration beyond two levels, potentially enhancing performance through access to a larger computational space and requiring fewer entangling gates for certain algorithms. Qudits have theoretically exhibited advantages through compact logical encoding (to overcome erasure and ternary errors) [8–10]), as well as enhancements in efficiency and fault tolerance [11–15]. In the field of quantum key distribution, studies suggest that qudits can increase the average raw key rates and improve robustness and reliability [16,17]. Regarding other applications, theoretical reports have proposed the use of qutrits, the simplest qudit system, to enhance quantum algorithms (e.g., Shor's factoring [18], Grover's search [19,20], and quantum Fourier transformation [21]),

quantum simulations [22], quantum cryptography [23,24], and quantum communication [25].

Discussions have also been extended to more fundamental problems, such as the Byzantine agreement [26], efficient Toffoli gates [27], and quantum channels demonstrating the superadditivity of classical capacity [28]. Certain quantum gates, such as parametrized gates for quantum heuristics [29], can be implemented more naturally in qutrit systems [30], as qutrits offer a more direct and efficient mapping for spin-1 models compared to traditional qubits. This direct mapping is particularly beneficial in studying phenomena like the Haldane gap and many-body localization in spin-1 chains [31–34]. The approach in Ref. [31] involves catalyzing the algorithm so that its evolution mimics a Heisenberg model in a delocalized phase, which demonstrates a speedup in finding the ground state of the random-field Ising model due to gap amplification, with promising scalability indications.

It is worth noting that the advantages mentioned above can be offset by the costs of implementing and operating qudits in real quantum applications. The universal gate set for qudits consists of single-qudit gates in the SU($d$) group and entangling two-qudit gates [35–37]. Recent efforts have demonstrated that the universal qudit gate set and their coherent control can be implemented in superconducting transmons [38–40], photonic circuits [41], and trapped ions [42,43]. However, implementing high-fidelity qudit-based circuits also presents challenges, mainly due to the increased complexity in the design, fabrication, and control of quantum systems with higher dimensions.

Towards improving the fidelity of qudit circuits, one direction could be to explore some algebraic relations between

*ogunkoya@fnal.gov
†peng398@pnnl.gov
‡ozguler@wisc.edu

012426-1

qudit circuits for the purpose of circuit compression and optimization, which would result in more fault-resilient performance. Similar exploration for the qubit-based circuits has recently become quite active [44–51]. For example, the Yang-Baxter equation (YBE), which was originally introduced in theoretical physics [52] and statistical mechanics [53], has recently been shown to have connections to topological entanglement, quantum entanglement, and quantum computational universality [54–61]. For example, proposals have been reported for efficiently checking YBE in quantum devices [60,62,63]. In our previous work [59], we proved that for some model systems, the two-qubit time propagator $\mathcal{R}_{\theta,\delta}$, parametrized by a rotation angle $\theta$ and a phase $\delta$, bears a similar algebraic form to the SU(2) solution of the YBE. Therefore, the turnover relationship (1.1) can hold as long as certain algebraic relations between the parameters on both sides are satisfied. Remarkably, this turnover relation can be utilized to compress the corresponding time evolution circuit to a depth that scales linearly with respect to the number of qubits:



$$\tag{1.1}$$

This observation then opens the question of whether these turnover relations can be generalized for quantum circuits with higher dimensions. Mathematically, there have been discussions on finding the high-dimension solutions to the generalized YBE [64–68]; however, numerical searching of these high-dimension solutions can be challenging. So far, in addition to the SU(2) solutions, only an $8 \times 8$ solution to a generalized YBE has been reported and used to generate the Greenberger-Horne-Zeillinger states [68]. In this paper, as an exploratory effort in this direction, we primarily focus on establishing a similar turnover relation that can be utilized for the efficient quantum simulation of the quantum time dynamics of the one-dimensional spin-1 Heisenberg model. In particular, a natural mapping of the spin-1 system's states onto the qutrit states leading to more straightforward or efficient quantum simulations allows us to efficiently search for (1) the existence of rigorous algebraic conditions for the similar turnover relations to hold and (2) a numerically efficient approach that can provide imprecise but sufficiently accurate turnover circuits in the absence of rigorous algebraic relations.

In the following sections, we first define some notations that will be used in this paper. Then, we show for some simple models that rigorous turnover relations do exist. Finally, for models without rigorous turnover relations, we propose a numerical recipe to achieve inexact but accurate enough qutrit circuit substitutes. The numerical recipe and the corresponding error analysis are provided for the three-qutrit circuit simulating the time dynamics of a three-site spin-1 Heisenberg model. We conclude this paper by offering some remarks on our future effort.

## II. NOTATIONS AND SPIN ALGEBRA

The closed-system dynamics of a one-dimensional array of level-$d$ variables is realized by $U(d^N)$ unitary matrices, where $N$ denotes the size of the system. Throughout this paper, however, we specifically treat qudits as spin $s = (d-1)/2$ quantum states and consider their time evolution with certain bilinear spin Hamiltonians.

We recall that for $d = 2$, $s = 1/2$ the spin operators, satisfying the SU(2) commutation algebra

$$[S^x, S^y] = iS^z, \quad [S^y, S^z] = iS^x, \quad [S^z, S^x] = iS^y, \tag{2.1}$$

are halves of the Pauli matrices:

$$X = \begin{pmatrix} 0 & 1 \\ 1 & 0 \end{pmatrix}, \quad Y = \begin{pmatrix} 0 & -i \\ i & 0 \end{pmatrix}, \quad Z = \begin{pmatrix} 1 & 0 \\ 0 & -1 \end{pmatrix}. \tag{2.2}$$

The SU(2) algebra allows a quadratic Casimir invariant:

$$(S^x)^2 + (S^y)^2 + (S^z)^2 = s(s+1)\mathbf{1}. \tag{2.3}$$

For three-level systems ($d = 3$, $s = 1$) the $z$-basis representation of the spin-1 operators becomes

$$S^x = \frac{1}{\sqrt{2}} \begin{pmatrix} 0 & 1 & 0 \\ 1 & 0 & 1 \\ 0 & 1 & 0 \end{pmatrix} = \frac{1}{\sqrt{2}}(X \oplus 0 + 0 \oplus X), \tag{2.4}$$

$$S^y = \frac{1}{\sqrt{2}} \begin{pmatrix} 0 & -i & 0 \\ i & 0 & -i \\ 0 & i & 0 \end{pmatrix} = \frac{1}{\sqrt{2}}(Y \oplus 0 + 0 \oplus Y), \tag{2.5}$$

$$S^z = \begin{pmatrix} 1 & 0 & 0 \\ 0 & 0 & 0 \\ 0 & 0 & -1 \end{pmatrix} = (Z \oplus 0 + 0 \oplus Z). \tag{2.6}$$

As an alternative to (2.4), (2.5), and (2.6), it is sometimes more convenient to use the adjoint representation of the spin operators [69]:

$$\tilde{S}^x = \begin{pmatrix} 0 & 0 & 0 \\ 0 & 0 & i \\ 0 & -i & 0 \end{pmatrix} = 0 \oplus (-Y), \tag{2.7}$$

$$\tilde{S}^y = \begin{pmatrix} 0 & 0 & i \\ 0 & 0 & 0 \\ -i & 0 & 0 \end{pmatrix} = P_y \tilde{S}^x P_y^\dagger, \tag{2.8}$$

$$\tilde{S}^z = \begin{pmatrix} 0 & i & 0 \\ -i & 0 & 0 \\ 0 & 0 & 0 \end{pmatrix} = P_z \tilde{S}^x P_z^\dagger \tag{2.9}$$

with permutation matrices $P_y$ and $P_z$ given by

$$P_y = \begin{pmatrix} 0 & 1 & 0 \\ 1 & 0 & 0 \\ 0 & 0 & 1 \end{pmatrix}, \quad P_z = \begin{pmatrix} 0 & 1 & 0 \\ 0 & 0 & 1 \\ 1 & 0 & 0 \end{pmatrix}, \tag{2.10}$$

and

$$(\tilde{S}^x)^2 = \text{diag}(0, 1, 1), \tag{2.11}$$

$$(\tilde{S}^y)^2 = \text{diag}(1, 0, 1), \tag{2.12}$$

$$(\tilde{S}^z)^2 = \text{diag}(1, 1, 0). \tag{2.13}$$

Similar to the SU(2) cases, $\{\tilde{S}^x, \tilde{S}^y, \tilde{S}^z\}$ follows the commutation algebra

$$[\tilde{S}^x, \tilde{S}^y] = i\tilde{S}^z, \quad [\tilde{S}^y, \tilde{S}^z] = i\tilde{S}^x, \quad [\tilde{S}^z, \tilde{S}^x] = i\tilde{S}^y \quad (2.14)$$

The two representations $\{S^x, S^y, S^z\}$ and $\{\tilde{S}^x, \tilde{S}^y, \tilde{S}^z\}$ are connected through the basis change between spherical and Cartesian coordinates:

$$\tilde{S}^a = U_+ S^a U_+^\dagger, \quad a = x, y, z \quad (2.15)$$

with

$$U_\pm = \frac{1}{\sqrt{2}} \begin{pmatrix} -1 & 0 & \pm 1 \\ +i & 0 & \pm i \\ 0 & \sqrt{2} & 0 \end{pmatrix}. \quad (2.16)$$

The basis change (2.15) does not affect the algebraic relations and the circuit substitutes established in the following sections.

Some algebraic relations of the spin-1 operators are worth mentioning. For example, for $n \geq 1$, we have

$$\begin{cases} (\tilde{S}^a)^{2n} = (\tilde{S}^a)^2 \\ (\tilde{S}^a)^{2n+1} = \tilde{S}^a \qquad \text{for } a \neq b \in \{x, y, z\}, \\ \tilde{S}^a \tilde{S}^b \tilde{S}^a = \mathbf{0}_3 \end{cases} \quad (2.17)$$

which implies

$$\mathcal{U}_x(\alpha) = \exp(-i\alpha \tilde{S}^x \otimes \tilde{S}^x)$$

$$= \mathbf{I}_9 - i\sin(\alpha)(\tilde{S}^x \otimes \tilde{S}^x) - 2\sin^2\left(\frac{\alpha}{2}\right)(\tilde{S}^x \otimes \tilde{S}^x)^2$$

$$= \begin{pmatrix} \mathbf{I}_3 & \mathbf{0}_3 & \mathbf{0}_3 \\ \mathbf{0}_3 & \mathbf{I}_3 - 2\left(\sin\left(\frac{\alpha}{2}\right)\tilde{S}^x\right)^2 & \sin(\alpha)\tilde{S}^x \\ \mathbf{0}_3 & -\sin(\alpha)\tilde{S}^x & \mathbf{I}_3 - 2\left(\sin\left(\frac{\alpha}{2}\right)\tilde{S}^x\right)^2 \end{pmatrix}, \quad (2.18)$$

$$\mathcal{U}_y(\alpha) = \exp(-i\alpha \tilde{S}^y \otimes \tilde{S}^y)$$

$$= \mathbf{I}_9 - i\sin(\alpha)(\tilde{S}^y \otimes \tilde{S}^y) - 2\sin^2\left(\frac{\alpha}{2}\right)(\tilde{S}^y \otimes \tilde{S}^y)^2$$

$$= \begin{pmatrix} \mathbf{I}_3 - 2\left(\sin\left(\frac{\alpha}{2}\right)\tilde{S}^y\right)^2 & \mathbf{0}_3 & \sin(\alpha)\tilde{S}^y \\ \mathbf{0}_3 & \mathbf{I}_3 & \mathbf{0}_3 \\ -\sin(\alpha)\tilde{S}^y & \mathbf{0}_3 & \mathbf{I}_3 - 2\left(\sin\left(\frac{\alpha}{2}\right)\tilde{S}^y\right)^2 \end{pmatrix}, \quad (2.19)$$

$$\mathcal{U}_z(\alpha) = \exp(-i\alpha \tilde{S}^z \otimes \tilde{S}^z)$$

$$= \mathbf{I}_9 - i\sin(\alpha)(\tilde{S}^z \otimes \tilde{S}^z) - 2\sin^2\left(\frac{\alpha}{2}\right)(\tilde{S}^z \otimes \tilde{S}^z)^2$$

$$= \begin{pmatrix} \mathbf{I}_3 - 2\left(\sin\left(\frac{\alpha}{2}\right)\tilde{S}^z\right)^2 & \sin(\alpha)\tilde{S}^z & \mathbf{0}_3 \\ -\sin(\alpha)\tilde{S}^z & \mathbf{I}_3 - 2\left(\sin\left(\frac{\alpha}{2}\right)\tilde{S}^z\right)^2 & \mathbf{0}_3 \\ \mathbf{0}_3 & \mathbf{0}_3 & \mathbf{I}_3 \end{pmatrix}, \quad (2.20)$$

where $\mathbf{I}_m$ denotes an $m \times m$ identity matrix and $\mathbf{0}_m$ denotes an $m \times m$ zero matrix. Notably, from (2.8) and (2.9)



$$(2.21)$$



$$(2.22)$$

A more interesting feature of $\mathcal{U}_a(\alpha)$ with $a \in \{x, y, z\}$ is that



$$(2.23)$$

## III. YANG-BAXTER-LIKE RELATIONS IN THE QUTRIT CIRCUIT

This section aims to search Yang-Baxter-type identities for qutrit circuits. Specifically, this means establishing a $(3^3 \times 3^3)$ matrix relation of the following type:

$$[\mathcal{R}_1(\alpha) \otimes \mathbf{I}_3][\mathbf{I}_3 \otimes \mathcal{R}_2(\beta)][\mathcal{R}_3(\gamma) \otimes \mathbf{I}_3]$$
$$= [\mathbf{I}_3 \otimes \mathcal{R}_4(\delta)][\mathcal{R}_5(\epsilon) \otimes \mathbf{I}_3][\mathbf{I}_3 \otimes \mathcal{R}_6(\zeta)] \quad (3.1)$$

where the Greek letters $\alpha$–$\zeta$ collectively denote continuous rotations that parametrize two-qutrit operators $\mathcal{R}_n$, defined as a product of $\mathcal{U}_a$'s ($a \in \{x, y, z\}$). The rotation angles on the left-hand side (LHS) of (3.1) are unrestricted; we require that for all values of $\alpha$, $\beta$, and $\gamma$ there should be a value of $\delta$, $\epsilon$, and $\zeta$ that satisfies (3.1). The parameters are typically related via unclosed expressions involving trigonometric functions, derived from elementwise equalities of (3.1). In the following subsections, we describe analytical and numerical methods to establish (3.1) with various $\mathcal{R}_n$'s.

### A. Simple turnover identities

We start from the simple case where $\mathcal{R}_n = \mathcal{U}_a$ for $a \in \{x, y, z\}$. If all the rotations are same, then by directly applying (2.23) to the LHS or right-hand side (RHS) of (3.1), we obtained the following YBEs relationships:

(1) LHS:



(2) RHS:



(3) LHS = RHS:



For more general cases where the rotations are not necessarily same, as explicitly shown in Appendix A, as long as the

following conditions are satisfied,

$$\begin{cases} \alpha + \gamma = \epsilon + 2k\pi \\ \delta + \zeta = \beta + 2k\pi \end{cases}, \quad k \in \mathbf{Z}, \qquad (3.2)$$

the identity (3.1) holds for all $\mathcal{U}_a$ ($a = x, y, z$). This can also be understood as an immediate consequence of the qubit relations. See Appendix B for the explanation.

The bonus identities can also be obtained from a simple observation: The spin matrices expressed in the adjoint representation also satisfy, for example,

$$U_\pm^\dagger \tilde{S}^y U_\pm = \frac{1}{\sqrt{2}}(-\tilde{S}^z \mp \tilde{S}^x). \qquad (3.3)$$

Other cyclic relations can further be obtained by utilizing (2.8) and (2.9). It can be shown that

$$V_\pm^\dagger \tilde{S}^x V_\pm = \frac{1}{\sqrt{2}}(-\tilde{S}^y \pm \tilde{S}^z), \qquad (3.4)$$

\vskip3pt

$$W_\pm^\dagger \tilde{S}^z W_\pm = \frac{1}{\sqrt{2}}(+\tilde{S}^x \mp \tilde{S}^y) \qquad (3.5)$$

with

$$V_\pm = \frac{1}{\sqrt{2}} \begin{pmatrix} 0 & +i & \pm i \\ 0 & \mp 1 & +1 \\ \sqrt{2} & 0 & 0 \end{pmatrix}, \qquad (3.6)$$

$$W_\pm = \frac{1}{\sqrt{2}} \begin{pmatrix} \mp 1 & +1 & 0 \\ 0 & 0 & \sqrt{2} \\ +i & \pm i & 0 \end{pmatrix}. \qquad (3.7)$$

Since the Yang-Baxter identity (3.1) is independent of the basis, it implies that $\mathcal{R}_n(\theta) \equiv \exp[i\theta(S^a \pm S^b) \otimes (S^a \pm S^b)]$ with any $a \neq b \in \{x, y, z\}$ also satisfies (3.1).

In the same way, we can derive the identity (3.1) for the following set of extended operators: $\mathcal{R}_n(\theta) = \exp[i\theta(S^x \pm S^y \pm S^z) \otimes (S^x \pm S^y \pm S^z)]$ with any choice of $\pm$ factors. This starts with observing the conjugation relation,

$$M_{\pm\pm}^\dagger \tilde{S}^z M_{\pm\pm} = \frac{1}{\sqrt{3}}(\tilde{S}^x \mp \tilde{S}^y \pm \tilde{S}^z), \qquad (3.8)$$

where

$$M_{s_1 s_2} = \frac{1}{\sqrt{6}} \begin{pmatrix} -s_1\sqrt{3}i & \sqrt{3}i & 0 \\ -s_2 i & -s_1 s_2 i & 2i \\ s_2\sqrt{2} & s_1 s_2\sqrt{2} & \sqrt{2} \end{pmatrix} \qquad (3.9)$$

for $s_1, s_2 \in \{\pm 1\}$. Note that the unitarity holds for $M_{\pm\pm}$, as for the other matrices in (2.16), (3.6), and (3.7). Thus, any fixed combination of $(S^x \pm S^y \pm S^z)$ can replace all $S^z$ that appear in the circuit identity (3.1) through $\mathcal{R}_n = \mathcal{U}_z$ if we insert the resolution of identity

$$M_{\pm\pm} M_{\pm\pm}^\dagger = \mathbf{I}_3$$

wherever needed.

The discussion so far has established the Yang-Baxter-type circuit relations (3.1) for the simple cases where it is assumed that all $\mathcal{R}$ operators have the same form

$$\mathcal{R}_n = \mathcal{U}_{s_x s_y s_z} \qquad (3.10)$$

and depend on a single continuous parameter, i.e.,

$$\mathcal{U}_{s_x s_y s_z}(\alpha) \equiv \exp\left[-i\alpha \left(\sum_{a \in \{x,y,z\}} s_a S^a\right)^{\otimes 2}\right] \qquad (3.11)$$

where $s_x, s_y, s_z \in \{+1, 0, -1\}$.

### B. Numerical methods for approximate identities

We remark that when establishing the circuit identity (3.1) analytically, numerical validation serves as a useful and efficient strategy to verify its correctness. This step involves evaluating the following expression:

$$\|(\mathcal{R}_1(\alpha) \otimes \mathbf{I}_3)(\mathbf{I}_3 \otimes \mathcal{R}_2(\beta))(\mathcal{R}_3(\gamma) \otimes \mathbf{I}_3)$$
$$- (\mathbf{I}_3 \otimes \mathcal{R}_4(\delta))(\mathcal{R}_5(\epsilon) \otimes \mathbf{I}_3)(\mathbf{I}_3 \otimes \mathcal{R}_6(\zeta))\| < \varepsilon \quad (3.12)$$

with a sufficiently small value of $\varepsilon$. The values for $\alpha, \beta, \gamma$, and $\delta$ are repeatedly sampled from a uniform distribution while $\epsilon$ and $\zeta$ follow from the constraint (3.2).

This numerical approach holds a broader range of applications and offers advantages in establishing approximate identities. While exact turnover relations may be specific to certain Hamiltonians, there are chances to develop approximate relations with tolerable levels of infidelity for a wider class of Hamiltonians. Such relations can lead to the compression of circuit depth, thus enhancing the overall fidelity of Trotter circuits running on imperfect hardware. We explore this scenario in the current section, using a concrete example of the spin-1 $XY$ Hamiltonian on three qutrits:

$$H_{\text{XY}} = -J \sum_{i=0}^{2} \left(\tilde{S}_i^x \tilde{S}_{i+1}^x + \tilde{S}_i^y \tilde{S}_{i+1}^y\right). \qquad (3.13)$$

The time evolution unitary of this Hamiltonian system can be written as

$$e^{-itH_{\text{XY}}} = e^{iJt \sum_{i=0}^{2} (\tilde{S}_i^x \otimes \tilde{S}_{i+1}^x + \tilde{S}_i^y \otimes \tilde{S}_{i+1}^y)} \qquad (3.14)$$

for which we consider a few available Trotter forms, and numerically explore if the approximate turnover relation (3.1) holds. Specifically, for each Trotterization scheme, we evaluate $W_L(\boldsymbol{\theta}_L)$ and $W_R(\boldsymbol{\theta}_R)$, both representing unitary operators for one Trotter step and its corresponding turnover counterpart, respectively. Afterwards, we minimize the infidelity between $W_L$ and $W_R$,

$$\mathcal{C}(\boldsymbol{\theta}_L, \boldsymbol{\theta}_R) = 1 - \frac{1}{(3^3)^2} \|\text{tr}(W_L W_R^\dagger)\|^2, \qquad (3.15)$$

by optimizing $\boldsymbol{\theta}_R$ for randomly selected values of $\boldsymbol{\theta}_L$. Note that the error analysis in (3.15) is state independent, and the fidelity function $\frac{1}{3^6}\|\text{tr}(W_L W_R^\dagger)\|^2$ is equivalent to the mean overlap function which is a reasonable figure of merit to quantify coherent errors.

The specific configurations of unitary pairs, $(W_L, W_R)$, that we compute to minimize the infidelity (3.15) for, are summarized in Fig. 1. Each row in the figure is related to the respective Trotter scheme for (3.14), described below:

$$T_1 = \lim_{n_b \to \infty} \left(\mathcal{U}_y^{1,2}(\theta)\mathcal{U}_y^{0,1}(\theta)\mathcal{U}_x^{1,2}(\theta)\mathcal{U}_x^{0,1}(\theta)\right)^{n_b}, \quad (3.16)$$

$$T_2 = \lim_{n_b \to \infty} \left(\mathcal{U}_y^{1,2}(\theta)\mathcal{U}_x^{1,2}(\theta)\mathcal{U}_y^{0,1}(\theta)\mathcal{U}_x^{0,1}(\theta)\right)^{n_b}, \quad (3.17)$$

| Unitary Pairs on Test ($W_L \to W_R$) | Description |
|---|---|
|  | Trotter scheme $T_1$ (3.16) |
|  | Trotter scheme $T_2$ (3.17) |
|  | Trotter scheme $T_3$ (3.18) |
|  | Trotter scheme $T_4$ (3.19) |
|  | Trotter scheme $T_5$ (3.20) |
|  | Trotter scheme $T_6$ (3.21) |
|  | An exact-in-principle identity used for setting up the lower bounds in the numerical tests. |

FIG. 1. A list of qutrit unitary pairs $W_L(\theta, \cdots, \theta)$ and $W_R(\boldsymbol{\theta}_R)$, for which we test the approximate circuit relations through numerical minimization of the infidelity function (3.15). The top six rows correspond to the circuit reflection for different Trotter schemes (3.16)–(3.21). While the unitaries in the bottom row are shown to be identical through (2.23), under the parameter constraint of (3.2), their equivalence is also tested numerically as a proxy to measure numerical deviations and limitations of optimizers.

$$T_3 = \lim_{n_b \to \infty} \left( \mathcal{U}_{x+y}^{1,2}(\theta) \mathcal{U}_{x+y}^{0,1}(\theta) \right)^{n_b}, \tag{3.18}$$

$$T_4 = \lim_{n_b \to \infty} \left( \mathcal{U}_{y}^{0,1}(\theta) \mathcal{U}_{x}^{1,2}(\theta) \mathcal{U}_{y}^{1,2}(\theta) \mathcal{U}_{x}^{0,1}(\theta) \right)^{n_b}, \tag{3.19}$$

$$T_5 = \lim_{n_b \to \infty} \left( \mathcal{U}_{y}^{1,2}(\theta) \mathcal{U}_{x}^{1,2}(\theta) \mathcal{U}_{x+y}^{0,1}(\theta) \right)^{n_b}, \tag{3.20}$$

$$T_6 = \lim_{n_b \to \infty} \left( \mathcal{U}_{y}^{0,1}(\theta) \mathcal{U}_{x+y}^{1,2}(\theta) \mathcal{U}_{x}^{0,1}(\theta) \right)^{n_b}, \tag{3.21}$$

where $\theta = t/n_b$ and

$$\mathcal{U}_{x}^{i,j}(\theta) = \exp\left( -i\theta \tilde{S}_i^x \otimes \tilde{S}_j^x \right),$$
$$\mathcal{U}_{y}^{i,j}(\theta) = \exp\left( -i\theta \tilde{S}_i^y \otimes \tilde{S}_j^y \right), \tag{3.22}$$
$$\mathcal{U}_{x+y}^{i,j}(\theta) = \exp\left( -i\theta \left( \tilde{S}_i^x \otimes \tilde{S}_j^x + \tilde{S}_i^y \otimes \tilde{S}_j^y \right) \right).$$

**(a) J = 0.10**

| $n_b$ | $T_1$ | $T_2$ | $T_3$ | $T_4$ | $T_5$ | $T_6$ | Exact |
|---|---|---|---|---|---|---|---|
| 1 | −11.96 | −10.72 | −12.23 | −11.48 | −12.07 | −11.24 | −12.4 |
| 2 | −10.12 | −10.86 | −11.29 | −11.04 | −11.08 | −10.41 | −11.19 |
| 3 | −10.1 | −10.55 | −1.77 | −10.31 | −10.65 | −9.84 | −10.57 |
| 4 | −10.06 | −10.74 | −1.77 | −10.03 | −10.58 | −10.05 | −10.08 |
| 5 | −10.04 | −10.12 | −1.77 | −10.06 | −2.54 | −2.54 | −10.26 |

**(b) J = 0.55**

| $n_b$ | $T_1$ | $T_2$ | $T_3$ | $T_4$ | $T_5$ | $T_6$ | Exact |
|---|---|---|---|---|---|---|---|
| 1 | −9.02 | −9.02 | −9.27 | −9.02 | −9.13 | −9.13 | −13.54 |
| 2 | −8.73 | −8.63 | −10.27 | −8.62 | −8.48 | −8.58 | −9.53 |
| 3 | −8.55 | −8.39 | −1.35 | −8.35 | −8.6 | −8.19 | −9.32 |
| 4 | −8.3 | −9.01 | −1.77 | −8.41 | −7.64 | −7.02 | −8.7 |
| 5 | −8.79 | −8.25 | −2.09 | −8.65 | −1.34 | −2.48 | −8.99 |

**(c) J = 1.00**

| $n_b$ | $T_1$ | $T_2$ | $T_3$ | $T_4$ | $T_5$ | $T_6$ | Exact |
|---|---|---|---|---|---|---|---|
| 1 | −7.98 | −7.98 | −8.23 | −7.98 | −8.09 | −8.09 | −12.88 |
| 2 | −7.79 | −7.7 | −7.55 | −7.66 | −7.54 | −7.61 | −9.06 |
| 3 | −7.6 | −8.18 | −1.77 | −7.79 | −7.18 | −6.96 | −7.82 |
| 4 | −7.76 | −8.22 | −1.77 | −8.43 | −6.89 | −6.34 | −7.87 |
| 5 | −7.33 | −8.67 | −1.95 | −8.04 | −6.38 | −1.35 | −7.7 |

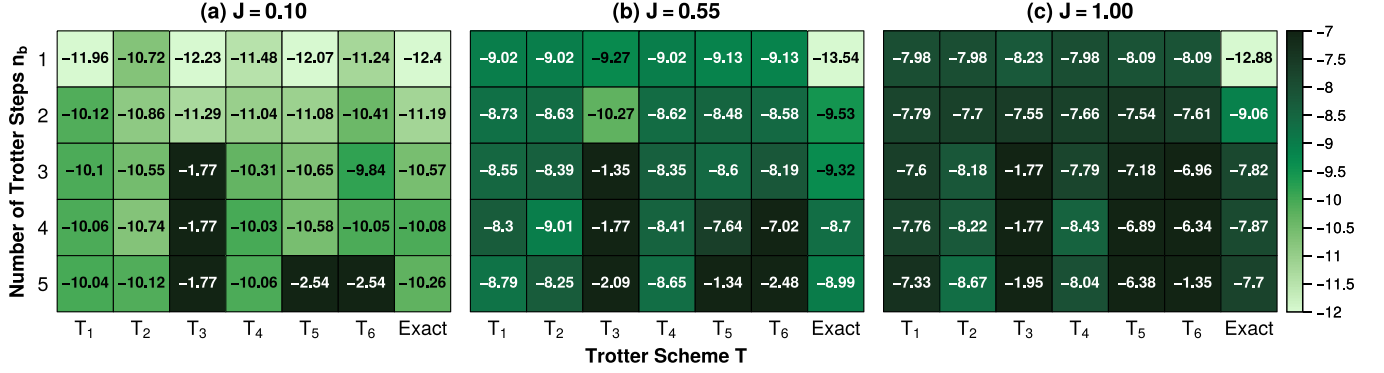Number of Trotter Steps $n_b$    Trotter Scheme T

FIG. 2. The minimized infidelity, $\log_{10} \min_{\theta_R} \mathcal{C}(\theta, \cdots, \theta, \theta_R)$, is obtained through parameter optimization of $\theta_R$ across various spin couplings $J \in \{0.1, 0.55, 1.0\}$ and Trotter schemes $T \in \{T_1, T_2, \cdots, T_6\}$. The displayed values are on the logarithmic base 10 scale. Circuit diagrams of parametrized unitaries $W_L(\theta, \cdots, \theta)$ and $W_R(\theta_R)$ for each Trotter scheme are shown in Fig. 1. The parameter optimization was performed using the BFGS algorithm. We consider the minimized infidelity to be reasonably low if it closely matches the "lower bound," which solely accounts for the numerical inaccuracy of the exact identity (3.23).

Although the Trotter unitaries live on a one-dimensional slice of the $\theta_L$-parameter space, i.e., $\theta_L = (\theta, \theta, \cdots)$, it is necessary to treat all components of $\theta_R$ independently in order to achieve a reasonably high fidelity. Therefore, we conduct numerical optimization for $\theta_R$ with the following configuration:

$$\min_{\theta_R} \mathcal{C}(\theta, \cdots, \theta, \theta_R) = \max_{\theta_R} \|\mathrm{tr}\,[W_L(\theta, \cdots, \theta)\, W_R^{\dagger}(\theta_R)]\|^2.$$

More generally, we consider numerical optimization using respective products of $n_b > 1$ instances of $W_L$ and $W_R$.

Our optimization results for infidelity are depicted in Fig. 2 across different values of spin-spin coupling $J \in \{0.10, 0.55, 1.00\}$. Each panel is associated with specific $J$ values and displays the minimized infidelities on a logarithmic scale for different Trotter schemes $\{T_1, \cdots, T_6\}$, covering a range of repetition numbers $1 \leqslant n_b \leqslant 5$. When benchmarking the infidelities between mirror-symmetric pairs of different candidate unitaries, it is necessary to establish a lower bound result that can represent practical expectations for the optimum, taking into account numerical deviations and limitations of optimizers. We achieve this through the following exact-in-principle circuit identity:

$$\mathcal{U}_y^{1,2}(\theta)\mathcal{U}_y^{0,1}(\theta)\mathcal{U}_x^{1,2}(\theta)\mathcal{U}_x^{0,1}(\theta)$$
$$= \mathcal{U}_y^{0,1}(\mu)\mathcal{U}_y^{1,2}(\sigma)\mathcal{U}_x^{0,1}(\zeta)\mathcal{U}_x^{1,2}(\lambda), \qquad (3.23)$$

where $\mu$, $\sigma$, $\zeta$, and $\lambda$ should in principle be equal to $\theta$, illustrated in the bottom row of Fig. 1. It is derived from the repeated application of the exact turnover relation (2.23). Therefore, its minimized infidelities should vanish ideally, i.e., $\min_{\theta_R} \mathcal{C}(\theta_L, \theta_R) = 0$ for any $\theta_L$, but are realistically sustained through the numerical optimizer at values ranging from $10^{-7}$ to $10^{-14}$ across different setups of $J$ and $n_b$, as depicted in Fig. 2.

In the upper six rows of Fig. 1, the reflection pairs of unitaries are strategically arranged so that their repeated application within the Trotter circuit leads to a substantial reduction in the total gate count. For instance, let us consider the Trotter scheme $T_1$ and its corresponding unitaries. The initial configuration involves 4 $\mathcal{U}_x$ and $\mathcal{U}_y$ operations for every Trotter step, summing up to a total of $4n$ gates. However, by replacing every alternating $W_L(\theta, \cdots, \theta)$ with $W_R(\mu, \sigma, \zeta, \lambda)$ at

precomputed values of $\mu$, $\sigma$, $\zeta$, and $\lambda$, it becomes possible to condense $(n-1)$ gates within intermediate Trotter layers due to subsequent applications of the same unitaries, namely,

$$\mathcal{U}_a^{i,j}(\theta_1)\mathcal{U}_a^{i,j}(\theta_2) = \mathcal{U}_a^{i,j}(\theta_1 + \theta_2) \text{ with } a \in \{x, y\}. \qquad (3.24)$$

This results in a reduced count of $(3n + 1)$ gates.

It is worth noting that further circuit compression is possible, but its feasibility depends on the numerical accuracy of the optimizer and the value of $J$. Consider the $T_3$ compression scheme, as illustrated in Eq. (3.18). Continuous compression could reduce the circuit depth to $O(1)$ if the turnover relation is exact. However, as observed in Fig. 2, such compression becomes possible only for $J = 0.1$, $n_b = 2$ and $J = 0.55$, $n_b = 2$, whose infidelity is even lower than that for the exact turnover identity. Since $n_b$ is flexible in this context, a direct comparison between two compression schemes with different $n_b$ values is inadequate. Another comparison must be conducted concerning the "numerical performance" of the analytically exact turnover relations. Figure 3 provides an example of two compression schemes with different $n_b$ values tested for $J = 1.0$. Despite Fig. 2 indicating a minor difference in infidelities between $T_2$ with $n_b = 5$ and $T_3$ with $n_b = 2$, which are $10^{-8.67}$ and $10^{-7.55}$ respectively, the former is lower and the latter is higher than the numerical infidelities for the exact turnover relations at their respective $n_b$ values. This discrepancy results in a noticeable difference in actual performance under the noiseless simulation, leading to significantly better accuracy for the $T_2$ scheme at $n_b = 5$.

Hence, to attain a computational advantage with the Trotter unitary, we select $T \in \{T_1, \cdots, T_6\}$ and $1 \leqslant n_b \leqslant 5$ based on initial calculations in Fig. 2, then apply the approximate relation $W_L^{n_b} \simeq W_R^{n_b}$ for every alternate set of $n_b$ Trotter steps. While replacing $W_L^{n_b}$ with $W_R^{n_b}$ may increase the overall infidelity of the Trotter circuit, the approximation error has a negligible impact when we use $T$ and $n_b$, whose corresponding infidelity from Fig. 2 stays at a level similar to the lower bound (3.23), i.e., the last column in each panel of Fig. 2.

Utilizing the infidelity metric outlined in (3.15), we derived a precise lower bound (see Appendix C) for the infidelity across multiple trotter steps compared to a single trotter step: $\mathcal{C}_{n_b}(\theta_L, \theta_R) \geqslant 1 - (1 - \mathcal{C}_1)^{n_b}$, where $\mathcal{C}_1$ is the infidelity for one
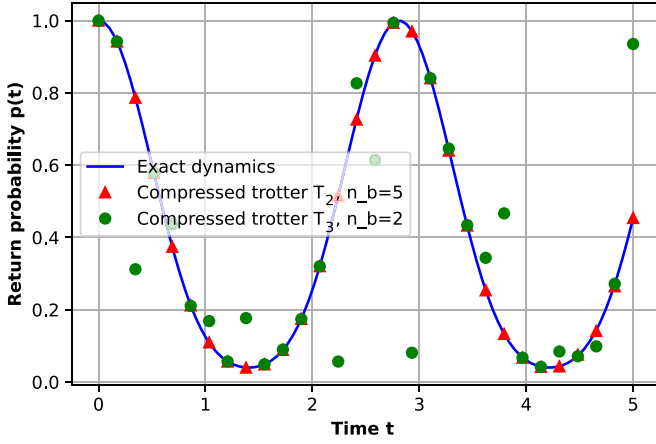
FIG. 3. The return probability (3.25) of the spin-1 XY model on a three-site lattice, starting and ending at the state $|202\rangle$, is displayed as a function of time within $0 \leqslant t < 5$. The spin coupling is set at $J = 1.0$. The best Trotter scheme $(T_2, n_b = 5)$ as from Fig. 2 is compared to another scheme $(T_3, n_b = 2)$, with its data points represented as red and green dots.

Trotter step and $n_b$ denotes the exact number of trotter steps. The sharpness of this lower bound incentivizes the minimizer to actively pursue it in each optimization process involving $n_b$ trotter steps. Consequently, deviations from this lower bound signal deficiencies in the minimizer's performance. As a precautionary measure, trotter forms associated with values significantly distant from this lower bound are deliberately excluded when choosing $T \in T_1, \ldots, T_6$.

As a pilot application, we evaluate the returning probability of the three-qutrit system as a function of time:

$$p(t) = \|\langle 202|e^{-itH_{XY}}|202\rangle\|^2 \qquad (3.25)$$

with the coupling constant $J = 0.1, 0.55, 1.0$. See the blue curve in Fig. 4 for the exact time evolution within $0 \leqslant t < 5$. Let us consider a Trotterization of (3.13) with the step size $\theta = 0.025$, resulting in a total of 200 steps. To employ the

above circuit compression strategy, it is crucial to select an appropriate Trotter scheme based on the benchmarking outcomes in Fig. 2. For example, we find that for $J = 0.55$, choosing $T = T_3$ and $n_b = 2$ corresponds to a sufficiently low infidelity, $10^{-10.27}$, even less than the numerical infidelity $(10^{-9.53})$ of the analytically exact turnover relation. We then impose the approximate reflection relation $W_L^2 \simeq W_R^2$ sequentially, by skipping the initial $W_L$ and then substituting the following $W_L^2$ with $W_R^2$. This process repeats by skipping the subsequent $W_L$ and replacing the next $W_L^2$ with $W_R^2$, until no more $W_L^2$ remains. For 200 Trotter blocks, the substitution is performed 66 times, leading to the consolidation of 132 $\mathcal{U}_{x+y}$ gates. We show the noiseless simulation results from the approximately compressed circuits as red triangles in Fig. 4. They demonstrate strong agreement, which is beneficial since it maintains the same level of numerical accuracy while reducing the usage of quantum resources on a qutrit-based quantum computer. All simulations for exact quantum time dynamics and its Trotterized version shown in Fig. 3 have been performed using the QUTIP package [70,71].

## IV. CONCLUSION AND OUTLOOK

In this paper, we extended the discussion of searching for Yang-Baxter-like turnover relations to qudit-based quantum computing. We explored certain algebraic properties of spin-1 operators and found rigorous Yang-Baxter-like turnover relations for simple qudit models. Regarding more complex qudit models, advanced algebraic relations are challenging to resolve rigorously, but a preliminary and plausible strategy is briefly discussed, based on the conjugation relation between the spin-1 operators. Nevertheless, since large-scale quantum simulation often requires an inexact but sufficiently accurate quantum simulation, we also placed an emphasis on the numerical exploration of advanced relations for the spin-1 system. As a demonstration, we examined the spin-1 XY model and numerically explored advanced circuit turnover relations in the quantum simulation of time dynamics. In particular, we designed a pool of circuit fragment turnover pairs using
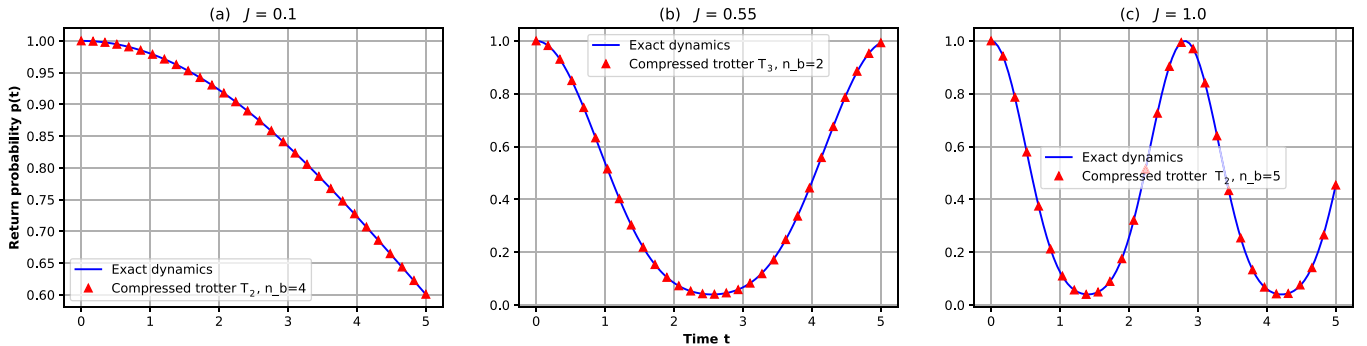


FIG. 4. The return probability (3.25) of the spin-1 XY model on a three-site lattice, starting and ending at the state $|202\rangle$, is shown as a function of time within $0 \leqslant t < 5$. Each plot corresponds to respective spin couplings $J = 0.1, 0.55, 1.0$. The dynamic simulation is represented as the blue line. We employ the Trotterization of the time-evolution operator (3.14) over 200 steps, with a corresponding step size of $\theta = 0.025$. Then we apply the circuit compression strategy detailed in Sec. III B to reduce the number of gates. For Trotter schemes $(T_3, n_b = 2)$, $(T_2, n_b = 4)$, and $(T_2, n_b = 5)$, the resulting data points are indicated by small red dots. More generally, for a $(T_3, n_b = 2)$ Trotter circuit with more than $n > 3$ steps, the approximate count of reduced gates is $2n/3$. For a $(T_2, n_b = 4)$ Trotter circuit with more than $n > 4$ steps, the approximate count of reduced gates is $\lfloor 2n/5 \rfloor - 1$. For a $(T_2, n_b = 5)$ Trotter circuit with more than $n > 5$ steps, the approximate count of reduced gates is $n/3 - 1$ when $n$ is a multiple of 6, and $2\lfloor n/6 \rfloor$ otherwise.

various Trotterization schemes and numerically examined their fidelity to screen out potential turnover pairs that could be utilized to optimize the deep circuit corresponding to many Trotter steps in the quantum dynamics simulations. Preliminary numerical demonstrations were given on the quantum simulation of the three-qutrit XY model, where the results from our proposed numerical scheme showed great agreement with the exact curve. Remarkably, our numerical scheme can be considered as a prototype of a machine learning process to be integrated into qubit control [72] and circuit compilation and optimization [73] and to improve our Yang-Baxter compiler QuYBE [56]. Specifically, the circuit optimization strategy can be boiled down to a combinatorial problem of searching for and performing circuit fragment turnovers in a given circuit with a layered structure, a task that can also be greatly facilitated by high-performance computing hardware and brute-force search methods. Further studies in this direction are now underway. Our eventual goal is to develop an efficient parallel Yang-Baxter compiler such as QuYBE [56], which can be used for the compression of a variety of quantum circuits, with the initial target on quantum dynamics circuits.

**APPENDIX A: DERIVATION OF THE TURNOVER IDENTITIES WITH $\mathcal{U}_x$, $\mathcal{U}_y$, AND $\mathcal{U}_z$**

Let $a = x$ and

$$
\mathcal{U}_x(\alpha) = \begin{pmatrix} \mathbf{I}_3 & \mathbf{0}_3 & \mathbf{0}_3 \\ \mathbf{0}_3 & \mathbf{I}_3 - 2\left(\sin\left(\frac{\alpha}{2}\right)\tilde{S}^x\right)^2 & \sin(\alpha)\tilde{S}^x \\ \mathbf{0}_3 & -\sin(\alpha)\tilde{S}^x & \mathbf{I}_3 - 2\left(\sin\left(\frac{\alpha}{2}\right)\tilde{S}^x\right)^2 \end{pmatrix}
\tag{A1}
$$

$$
= \begin{pmatrix} \mathbf{I}_3 & \mathbf{0}_3 & \mathbf{0}_3 \\ \mathbf{0}_3 & \mathbf{A}_\alpha & \mathbf{B}_\alpha \\ \mathbf{0}_3 & -\mathbf{B}_\alpha & \mathbf{A}_\alpha \end{pmatrix}
\tag{A2}
$$

where we denote

$$
\mathbf{A}_\alpha = \mathbf{I}_3 - 2\left(\sin\left(\frac{\alpha}{2}\right)\tilde{S}^x\right)^2,
\tag{A3}
$$

$$
\mathbf{B}_\alpha = \sin(\alpha)\tilde{S}^x.
\tag{A4}
$$

Now taking the LHS of (3.1) and replace $\mathcal{R}_n$ with $\mathcal{U}_x$, it is straightforward to show that

$$
(\mathcal{U}_x(\alpha) \otimes \mathbf{I}_3)(\mathbf{I}_3 \otimes \mathcal{U}_x(\beta))(\mathcal{U}_x(\gamma) \otimes \mathbf{I}_3) = \begin{pmatrix} \mathbf{I}_9 & \mathbf{0}_9 & \mathbf{0}_9 \\ \mathbf{0}_9 & \mathbf{A}_\alpha \otimes \mathbf{I}_3 & \mathbf{B}_\alpha \otimes \mathbf{I}_3 \\ \mathbf{0}_9 & -\mathbf{B}_\alpha \otimes \mathbf{I}_3 & \mathbf{A}_\alpha \otimes \mathbf{I}_3 \end{pmatrix} \begin{pmatrix} \mathcal{U}_x(\beta) & \mathbf{0}_9 & \mathbf{0}_9 \\ \mathbf{0}_9 & \mathcal{U}_x(\beta) & \mathbf{0}_9 \\ \mathbf{0}_9 & \mathbf{0}_9 & \mathcal{U}_x(\beta) \end{pmatrix} \begin{pmatrix} \mathbf{I}_9 & \mathbf{0}_9 & \mathbf{0}_9 \\ \mathbf{0}_9 & \mathbf{A}_\gamma \otimes \mathbf{I}_3 & \mathbf{B}_\gamma \otimes \mathbf{I}_3 \\ \mathbf{0}_9 & -\mathbf{B}_\gamma \otimes \mathbf{I}_3 & \mathbf{A}_\gamma \otimes \mathbf{I}_3 \end{pmatrix}
$$

$$
= \begin{pmatrix} \mathcal{U}_x(\beta) & \mathbf{0}_9 & \mathbf{0}_9 \\ \mathbf{0}_9 & \mathbf{C} & \mathbf{D} \\ \mathbf{0}_9 & -\mathbf{D} & \mathbf{C,} \end{pmatrix}
\tag{A5}
$$

with

$$
\mathbf{C} = (\mathbf{A}_\alpha \otimes \mathbf{I}_3)\mathcal{U}_x(\beta)(\mathbf{A}_\gamma \otimes \mathbf{I}_3) - (\mathbf{B}_\alpha \otimes \mathbf{I}_3)\mathcal{U}_x(\beta)(\mathbf{B}_\gamma \otimes \mathbf{I}_3),
\tag{A6}
$$

$$
\mathbf{D} = (\mathbf{A}_\alpha \otimes \mathbf{I}_3)\mathcal{U}_x(\beta)(\mathbf{B}_\gamma \otimes \mathbf{I}_3) + (\mathbf{B}_\alpha \otimes \mathbf{I}_3)\mathcal{U}_x(\beta)(\mathbf{A}_\gamma \otimes \mathbf{I}_3).
\tag{A7}
$$

Similarly, for the RHS of (3.1), we have

$$
(\mathbf{I}_3 \otimes \mathcal{U}_x(\delta))(\mathcal{U}_x(\epsilon) \otimes \mathbf{I}_3)(\mathbf{I}_3 \otimes \mathcal{U}_x(\zeta)) = \begin{pmatrix} \mathcal{U}_x(\delta) & \mathbf{0}_9 & \mathbf{0}_9 \\ \mathbf{0}_9 & \mathcal{U}_x(\delta) & \mathbf{0}_9 \\ \mathbf{0}_9 & \mathbf{0}_9 & \mathcal{U}_x(\delta) \end{pmatrix} \begin{pmatrix} \mathbf{I}_3 & \mathbf{0}_3 & \mathbf{0}_3 \\ \mathbf{0}_3 & \mathbf{A}_\epsilon & \mathbf{B}_\epsilon \\ \mathbf{0}_3 & -\mathbf{B}_\epsilon & \mathbf{A}_\epsilon \end{pmatrix} \begin{pmatrix} \mathcal{U}_x(\zeta) & \mathbf{0}_9 & \mathbf{0}_9 \\ \mathbf{0}_9 & \mathcal{U}_x(\zeta) & \mathbf{0}_9 \\ \mathbf{0}_9 & \mathbf{0}_9 & \mathcal{U}_x(\zeta) \end{pmatrix}
$$

$$
= \begin{pmatrix} \mathcal{U}_x(\delta + \zeta) & \mathbf{0}_9 & \mathbf{0}_9 \\ \mathbf{0}_9 & \mathcal{U}_x(\delta)\mathbf{A}_\epsilon\mathcal{U}_x(\zeta) & \mathcal{U}_x(\delta)\mathbf{B}_\epsilon\mathcal{U}_x(\zeta) \\ \mathbf{0}_9 & -\mathcal{U}_x(\delta)\mathbf{B}_\epsilon\mathcal{U}_x(\zeta) & \mathcal{U}_x(\delta)\mathbf{A}_\epsilon\mathcal{U}_x(\zeta) \end{pmatrix}.
\tag{A8}
$$

Comparing (A5) with (A8), for (3.1) to hold, the following conditions need to be satisfied:

$$\mathcal{U}_x(\beta) = \mathcal{U}_x(\delta + \zeta), \tag{A9}$$

$$\mathbf{C} = \mathcal{U}_x(\delta)\mathbf{A}_\epsilon\mathcal{U}_x(\zeta), \tag{A10}$$

$$\mathbf{D} = \mathcal{U}_x(\delta)\mathbf{B}_\epsilon\mathcal{U}_x(\zeta). \tag{A11}$$

It is easy to see that (A9) is satisfied as long as

$$\beta + 2k\pi = \delta + \zeta, \quad k \in \mathbb{Z}. \tag{A12}$$

In (A10)

$$(\mathbf{A}_\alpha \otimes \mathbf{I}_3)\mathcal{U}_x(\beta)(\mathbf{A}_\gamma \otimes \mathbf{I}_3)$$

$$= \left(\mathbf{I}_9 - 2\sin^2\left(\frac{\alpha}{2}\right)(\tilde{S}^x)^2 \otimes \mathbf{I}_3)\right)\left(\mathbf{I}_9 - i\sin(\beta)(\tilde{S}^x \otimes \tilde{S}^x) - 2\sin^2\left(\frac{\beta}{2}\right)(\tilde{S}^x \otimes \tilde{S}^x)^2\right)\left(\mathbf{I}_9 - 2\sin^2\left(\frac{\gamma}{2}\right)(\tilde{S}^x)^2 \otimes \mathbf{I}_3)\right)$$

$$= \mathbf{I}_9 + (\cos(\alpha)\cos(\gamma) - 1)(\tilde{S}^x \otimes \mathbf{I}_3)^2 - i\cos(\alpha)\sin(\beta)\cos(\gamma)(\tilde{S}^x \otimes \tilde{S}^x) - 2\cos(\alpha)\sin^2\left(\frac{\beta}{2}\right)\cos(\gamma)(\tilde{S}^x \otimes \tilde{S}^x)^2, \tag{A13}$$

$$(\mathbf{B}_\alpha \otimes \mathbf{I}_3)\mathcal{U}_x(\beta)(\mathbf{B}_\gamma \otimes \mathbf{I}_3)$$

$$= (\sin(\alpha)(\tilde{S}^x \otimes \mathbf{I}_3))\left(\mathbf{I}_9 - i\sin(\beta)(\tilde{S}^x \otimes \tilde{S}^x) - 2\sin^2\left(\frac{\beta}{2}\right)(\tilde{S}^x \otimes \tilde{S}^x)^2\right)(\sin(\gamma)(\tilde{S}^x \otimes \mathbf{I}_3))$$

$$= \sin(\alpha)\sin(\gamma)(\tilde{S}^x \otimes \mathbf{I}_3)^2 - i\sin(\alpha)\sin(\beta)\sin(\gamma)(\tilde{S}^x \otimes \tilde{S}^x) - 2\sin(\alpha)\sin^2\left(\frac{\beta}{2}\right)\sin(\gamma)(\tilde{S}^x \otimes \tilde{S}^x)^2 \tag{A14}$$

$$\Rightarrow \mathbf{C} = \mathbf{I}_9 + (\cos(\alpha + \gamma) - 1)(\tilde{S}^x \otimes \mathbf{I}_3)^2 - i\cos(\alpha + \gamma)\sin(\beta)(\tilde{S}^x \otimes \tilde{S}^x) - \cos(\alpha + \gamma)(\cos(\beta) - 1)(\tilde{S}^x \otimes \tilde{S}^x)^2, \tag{A15}$$

$$\mathcal{U}_x(\delta)\mathbf{A}_\epsilon\mathcal{U}_x(\zeta) = \left(\mathbf{I}_9 - i\sin(\delta)(\tilde{S}^x \otimes \tilde{S}^x) - 2\sin^2\left(\frac{\delta}{2}\right)(\tilde{S}^x \otimes \tilde{S}^x)^2\right)\left(\mathbf{I}_9 - 2\sin^2\left(\frac{\epsilon}{2}\right)(\tilde{S}^x)^2 \otimes \mathbf{I}_3)\right)$$

$$\times \left(\mathbf{I}_9 - i\sin(\zeta)(\tilde{S}^x \otimes \tilde{S}^x) - 2\sin^2\left(\frac{\zeta}{2}\right)(\tilde{S}^x \otimes \tilde{S}^x)^2\right)$$

$$= \mathbf{I}_9 + (\cos(\epsilon) - 1)(\tilde{S}^x \otimes \mathbf{I}_3)^2 - i\cos(\epsilon)\sin(\delta + \zeta)(\tilde{S}^x \otimes \tilde{S}^x) + \cos(\epsilon)(\cos(\delta + \zeta) - 1)(\tilde{S}^x \otimes \tilde{S}^x)^2. \tag{A16}$$

Similarly, in (A11)

$$(\mathbf{A}_\alpha \otimes \mathbf{I}_3)\mathcal{U}_x(\beta)(\mathbf{B}_\gamma \otimes \mathbf{I}_3)$$

$$= \left(\mathbf{I}_9 - 2\sin^2\left(\frac{\alpha}{2}\right)(\tilde{S}^x)^2 \otimes \mathbf{I}_3)\right)\left(\mathbf{I}_9 - i\sin(\beta)(\tilde{S}^x \otimes \tilde{S}^x) - 2\sin^2\left(\frac{\beta}{2}\right)(\tilde{S}^x \otimes \tilde{S}^x)^2\right)(\sin(\gamma)(\tilde{S}^x \otimes \mathbf{I}_3))$$

$$= \cos(\alpha)\sin(\gamma)(\tilde{S}^x \otimes \mathbf{I}_3) - i\cos(\alpha)\sin(\beta)\sin(\gamma)((\tilde{S}^x)^2 \otimes \tilde{S}^x) - 2\cos(\alpha)\sin^2\left(\frac{\beta}{2}\right)\sin(\gamma)(\tilde{S}^x \otimes (\tilde{S}^x)^2), \tag{A17}$$

$$(\mathbf{B}_\alpha \otimes \mathbf{I}_3)\mathcal{U}_x(\beta)(\mathbf{A}_\gamma \otimes \mathbf{I}_3)$$

$$= (\sin(\alpha)(\tilde{S}^x \otimes \mathbf{I}_3))\left(\mathbf{I}_9 - i\sin(\beta)(\tilde{S}^x \otimes \tilde{S}^x) - 2\sin^2\left(\frac{\beta}{2}\right)(\tilde{S}^x \otimes \tilde{S}^x)^2\right)(\mathbf{I}_9 - 2\sin^2(\frac{\gamma}{2})(\tilde{S}^x)^2 \otimes \mathbf{I}_3))$$

$$= \sin(\alpha)\cos(\gamma)(\tilde{S}^x \otimes \mathbf{I}_3) - i\sin(\alpha)\sin(\beta)\cos(\gamma)((\tilde{S}^x)^2 \otimes \tilde{S}^x) - 2\sin(\alpha)\sin^2\left(\frac{\beta}{2}\right)\cos(\gamma)(\tilde{S}^x \otimes (\tilde{S}^x)^2) \tag{A18}$$

$$\Rightarrow \quad \mathbf{D} = \sin(\alpha + \gamma)(\tilde{S}^x \otimes \mathbf{I}_3) - i\sin(\alpha + \gamma)\sin(\beta)((\tilde{S}^x)^2 \otimes \tilde{S}^x) + \sin(\alpha + \gamma)(\cos(\beta) - 1)(\tilde{S}^x \otimes (\tilde{S}^x)^2), \tag{A19}$$

$$\mathcal{U}_x(\delta)\mathbf{B}_\epsilon\mathcal{U}_x(\zeta)$$

$$= \left(\mathbf{I}_9 - i\sin(\delta)(\tilde{S}^x \otimes \tilde{S}^x) - 2\sin^2\left(\frac{\delta}{2}\right)(\tilde{S}^x \otimes \tilde{S}^x)^2\right)(\sin(\epsilon)(\tilde{S}^x \otimes \mathbf{I}_3))\left(\mathbf{I}_9 - i\sin(\zeta)(\tilde{S}^x \otimes \tilde{S}^x) - 2\sin^2\left(\frac{\zeta}{2}\right)(\tilde{S}^x \otimes \tilde{S}^x)^2\right)$$

$$= \sin(\epsilon)(\tilde{S}^x \otimes \mathbf{I}_3) - i\sin(\epsilon)\sin(\delta + \zeta)((\tilde{S}^x)^2 \otimes \tilde{S}^x) + \sin(\epsilon)(\cos(\delta + \zeta) - 1)(\tilde{S}^x \otimes (\tilde{S}^x)^2). \tag{A20}$$

After a term-by-term comparison, one can see that the following conditions need to be satisfied,

$$\begin{cases} \alpha + \gamma = \epsilon + 2k\pi \\ \delta + \zeta = \beta + 2k\pi \end{cases}, \quad k \in \mathbb{Z}, \tag{A21}$$

for the following equation to hold:

$$(\mathcal{U}_x(\alpha) \otimes \mathbf{I}_3)(\mathbf{I}_3 \otimes \mathcal{U}_x(\beta))(\mathcal{U}_x(\gamma) \otimes \mathbf{I}_3) = (\mathbf{I}_3 \otimes \mathcal{U}_x(\delta))(\mathcal{U}_x(\epsilon) \otimes \mathbf{I}_3)(\mathbf{I}_3 \otimes \mathcal{U}_x(\zeta)). \tag{A22}$$

From (2.21) a further proof can be obtained for $a = y$:

$$
\begin{aligned}
(\mathcal{U}_y(\alpha) &\otimes \mathbf{I}_3)(\mathbf{I}_3 \otimes \mathcal{U}_y(\beta))(\mathcal{U}_y(\gamma) \otimes \mathbf{I}_3) \\
&= ((P_y \otimes P_y \otimes \mathbf{I}_3)(\mathcal{U}_x(\alpha) \otimes \mathbf{I}_3)(P_y \otimes P_y \otimes \mathbf{I}_3))((\mathbf{I}_3 \otimes P_y \otimes P_y)(\mathbf{I}_3 \otimes \mathcal{U}_x(\beta))(\mathbf{I}_3 \otimes P_y \otimes P_y)) \\
&\quad \times ((P_y \otimes P_y \otimes \mathbf{I}_3)(\mathcal{U}_x(\gamma) \otimes \mathbf{I}_3)(P_y \otimes P_y \otimes \mathbf{I}_3)) \\
&= (P_y \otimes P_y \otimes P_y)(\mathcal{U}_x(\alpha) \otimes \mathbf{I}_3)(\mathbf{I}_3 \otimes \mathcal{U}_x(\beta))(\mathcal{U}_x(\gamma) \otimes \mathbf{I}_3)(P_y \otimes P_y \otimes P_y) \\
&= (P_y \otimes P_y \otimes P_y)(\mathbf{I}_3 \otimes \mathcal{U}_x(\delta))(\mathcal{U}_x(\epsilon) \otimes \mathbf{I}_3)(\mathbf{I}_3 \otimes \mathcal{U}_x(\zeta))(P_y \otimes P_y \otimes P_y) \\
&= ((\mathbf{I}_3 \otimes P_y \otimes P_y)(\mathbf{I}_3 \otimes \mathcal{U}_x(\beta))(\mathbf{I}_3 \otimes P_y \otimes P_y))((P_y \otimes P_y \otimes \mathbf{I}_3)(\mathcal{U}_x(\alpha) \otimes \mathbf{I}_3)(P_y \otimes P_y \otimes \mathbf{I}_3)) \\
&\quad ((\mathbf{I}_3 \otimes P_y \otimes P_y)(\mathbf{I}_3 \otimes \mathcal{U}_x(\beta))(\mathbf{I}_3 \otimes P_y \otimes P_y)) \\
&= (\mathbf{I}_3 \otimes \mathcal{U}_y(\delta))(\mathcal{U}_y(\epsilon) \otimes \mathbf{I}_3)(\mathbf{I}_3 \otimes \mathcal{U}_y(\zeta)). \tag{A23}
\end{aligned}
$$

A similar process can be followed from (2.22) for the proof for $a = z$.

## APPENDIX B: QUTRIT IDENTITIES FROM QUBIT IDENTITIES

The adjoint spin-1 matrices $\tilde{S}^a$ can be seen as a $2 \times 2$ block embedding of Pauli $Y$ into a $3 \times 3$ matrix, implying that the unitaries $\mathcal{U}_a$ primarily affect only two levels of the qutrit. We can build a permutation $P$ that separates the spectator levels from the levels actively involved in the unitary operations.

Taking $\tilde{S}_x$ as an example, from (2.7) we have

$$
P = \begin{pmatrix}
4 & 5 & 6 & 10 & 11 & 12 & 13 & 14 & 15 & 16 & 17 & 18 & 19 & 20 & 21 & 22 & 23 & 24 \\
5 & 6 & 4 & 11 & 12 & 15 & 19 & 20 & 16 & 21 & 22 & 10 & 13 & 14 & 17 & 23 & 24 & 18
\end{pmatrix}
$$

which rearranges all three-qutrit states into the following direct sum between subspaces: $|000\rangle \oplus |00a\rangle \oplus |0a0\rangle \oplus |0ab\rangle \oplus |a00\rangle \oplus |a0b\rangle \oplus |ab0\rangle \oplus |abc\rangle$ with $a, b, c \in \{1, 2\}$. Such permutation decomposes the two-qutrit unitary action $\mathcal{U}_x$ into the direct sum $\mathbf{1}_1 \oplus \exp(-i\alpha Y_1) \oplus \exp(-i\alpha Y_2) \oplus \exp(-i\alpha Y_1 \otimes Y_2)$ where $Y_{1,2}$ act on effective "qubits" obtained from restricting qutrits onto the two levels $|1\rangle$ and $|2\rangle$.

Applying the above permutation to the qutrit turnover relation for $\mathcal{U}_x$, both sides of (2.23) take a block-diagonal form corresponding to some circuit identities on effective two-level systems.

(1) $|000\rangle$: The identity $1 = 1$ holds trivially.

(2) $|00a\rangle$: $e^{-i\alpha Y_3} = e^{-i\delta Y_3} e^{-i\zeta Y_3}$.

(3) $|0a0\rangle$: $e^{-i\alpha Y_2} e^{-i\beta Y_2} e^{-i\gamma Y_2} = e^{-i\delta Y_2} e^{-i\epsilon Y_2} e^{-i\zeta Y_2}$.

(4) $|a00\rangle$: $e^{-i\alpha Y_1} e^{-i\gamma Y_1} = e^{-i\epsilon Y_1}$.

(5) $|a0b\rangle$: $e^{-i\alpha Y_1} e^{-i\beta Y_3} e^{-i\gamma Y_1} = e^{-i\delta Y_3} e^{-i\epsilon Y_1} e^{-i\zeta Y_3}$.

(6) $|0ab\rangle$: $e^{-i\alpha Y_2} e^{-i\beta Y_2 \otimes Y_3} e^{-i\gamma Y_2} = e^{-i\delta Y_2 \otimes Y_3} e^{-i\epsilon Y_2} e^{-i\zeta Y_2 \otimes Y_3}$.

(7) $|ab0\rangle$: $e^{-i\alpha Y_1 \otimes Y_2} e^{-i\beta Y_2} e^{-i\gamma Y_1 \otimes Y_2} = e^{-i\delta Y_2} e^{-i\epsilon Y_1 \otimes Y_2} e^{-i\zeta Y_2}$.

(8) $|abc\rangle$: It returns the qubit turnover relation of [59].

The relations on $|00a\rangle$, $|0a0\rangle$, $|a00\rangle$, and $|a0b\rangle$ subspaces are obviously true if the circuit parameters satisfy (3.2). The $|0ab\rangle$ and $|ab0\rangle$ relations are also straightforward to verify since $[e^{-iuY_i}, e^{-ivY_i \otimes Y_j}] = 0$. The only remaining nontrivial circuit relation comes from the subspace $|abc\rangle$, equivalent to the "qubit" turnover relation shown in Ref. [59].

## APPENDIX C: LOWER BOUND OF THE INFIDELITY IN MULTIPLE TROTTER STEPS

In Fig. 2, we reported the numerical infidelities that we obtained from minimization. To evaluate the quality of the minimization which may compromise the infidelity, we can compute the lower bound of the infidelity. Similar to Eq. (3.15), given a Trotter scheme, for $n_b$ Trotter steps, the infidelity can be generalized to

$$\mathcal{C}_{n_b}(\boldsymbol{\theta}_L, \boldsymbol{\theta}_R) = 1 - \frac{1}{(3^3)^{2n_b}} \|\mathrm{tr}\,[(W_L)^{n_b}(W_R^\dagger)^{n_b}]\|^2. \tag{C1}$$

If $W_L W_R^\dagger$ is positive semidefinite (which can be generally true when $W_L W_R^\dagger \to I$), we then have

$$
\begin{aligned}
\mathrm{tr}\,[(W_L)^{n_b}(W_R^\dagger)^{n_b}] &= \mathrm{tr}\,[(W_L W_R^\dagger)^{n_b}] \\
&\leqslant [\mathrm{tr}\,(W_L W_R^\dagger)]^{n_b}, \tag{C2}
\end{aligned}
$$

and the lower bound of (C1) can be expressed as

$$
\begin{aligned}
\mathcal{C}_{n_b} &\geqslant 1 - \left[\frac{1}{(3^3)^2}\|\mathrm{tr}\,(W_L W_R^\dagger)\|^2\right]^{n_b} \\
&= 1 - (1 - \mathcal{C}_1)^{n_b}. \tag{C3}
\end{aligned}
$$

Here $\mathcal{C}_1$ is the infidelity for one Trotter step. Now based on the computed lower bounds, we can evaluate the minimized infidelities reported in Fig. 2. In particular, if the minimized infidelity is far away from the computed lower bound such as T3 ($n_b \geqslant 3$), the minimization becomes deficient.

[1] D. P. DiVincenzo, Two-bit gates are universal for quantum computation, Phys. Rev. A **51**, 1015 (1995).

[2] S. B. Bravyi and A. Yu. Kitaev, Quantum codes on a lattice with boundary, arXiv:quant-ph/9811052.

[3] E. Dennis, A. Kitaev, A. Landahl, and J. Preskill, Topological quantum memory, J. Math. Phys. **43**, 4452 (2002).

[4] Z. Chen, K. J. Satzinger, J. Atalaya, A. N. Korotkov, A. Dunsworth, D. Sank, C. Quintana, M. McEwen, R. Barends, P. V. Klimov *et al.*, Exponential suppression of bit or phase errors with cyclic error correction, Nature (London) **595**, 600 (2021).

[5] S. Krinner, N. Lacroix, A. Remm, A. D. Paolo, E. Genois, C. Leroux, C. Hellings, S. Lazar, F. Swiadek, J. Herrmann *et al.*, Realizing repeated quantum error correction in a distance-three surface code, Nature (London) **605**, 669 (2022).

[6] J. F. Marques, B. M. Varbanov, M. S. Moreira, H. Ali, N. Muthusubramanian, C. Zachariadis, F. Battistel, M. Beekman, N. Haider, W. Vlothuizen *et al.*, Logical-qubit operations in an error-detecting surface code, Nat. Phys. **18**, 80 (2022).

[7] Y. Zhao, Y. Ye, H.-L. Huang, Y. Zhang, D. Wu, H. Guan, Q. Zhu, Z. Wei, T. He, S. Cao *et al.*, Realization of an error-correcting surface code with superconducting qubits, Phys. Rev. Lett. **129**, 030501 (2022).

[8] E. Kapit, Hardware-efficient and fully autonomous quantum error correction in superconducting circuits, Phys. Rev. Lett. **116**, 150501 (2016).

[9] R. Majumdar, S. Basu, S. Ghosh, and S. Sur-Kolay, Quantum error-correcting code for ternary logic, Phys. Rev. A **97**, 052302 (2018).

[10] S. Muralidharan, C.-L. Zou, L. Li, J. Wen, and L. Jiang, Overcoming erasure errors with multilevel systems, New J. Phys. **19**, 013026 (2017).

[11] M. Alam, S. Belomestnykh, N. Bornman, G. Cancelo, Y.-C. Chao, M. Checchin, V. S. Dinh, A. Grassellino, E. J. Gustafson, R. Harnik *et al.*, Quantum computing hardware for HEP algorithms and sensing, TBD (2022), https://www.osti.gov/biblio/1864203.

[12] E. T. Campbell, Enhanced fault-tolerant quantum computing in *d*-level systems, Phys. Rev. Lett. **113**, 230501 (2014).

[13] E. T. Campbell, H. Anwar, and D. E. Browne, Magic-state distillation in all prime dimensions using quantum reed-muller codes, Phys. Rev. X **2**, 041021 (2012).

[14] M. Otten, K. Kapoor, A. B. Özgüler, E. T. Holland, J. B. Kowalkowski, Y. Alexeev, and A. L. Lyon, Impacts of noise and structure on quantum information encoded in a quantum memory, Phys. Rev. A **104**, 012605 (2021).

[15] A. B. Özgüler and J. A. Job, Dynamics of qudit gates and effects of spectator modes on optimal control pulses, arXiv:2207.14006.

[16] T. Durt, N. J. Cerf, N. Gisin, and M. Żukowski, Security of quantum key distribution with entangled qutrits, Phys. Rev. A **67**, 012311 (2003).

[17] S. P. Walborn, D. S. Lemelle, M. P. Almeida, and P. H. S. Ribeiro, Quantum key distribution with higher-order alphabets using spatially encoded qudits, Phys. Rev. Lett. **96**, 090501 (2006).

[18] A. Bocharov, M. Roetteler, and K. M. Svore, Factoring with qutrits: Shor's algorithm on ternary and metaplectic quantum architectures, Phys. Rev. A **96**, 012306 (2017).

[19] S. S. Bullock, D. P. O'Leary, and G. K. Brennen, Asymptotically optimal quantum circuits for *d*-level systems, Phys. Rev. Lett. **94**, 230502 (2005).

[20] P. Gokhale, J. M. Baker, C. Duckering, N. C. Brown, K. R. Brown, and F. T. Chong, Asymptotic improvements to quantum circuits via qutrits, in *Proceedings of the 46th International Symposium on Computer Architecture* (Association for Computing Machinery, New York, 2019), pp. 554–566.

[21] A. Pavlidis and E. Floratos, Quantum-fourier-transform-based quantum arithmetic with qudits, Phys. Rev. A **103**, 032417 (2021).

[22] E. Gustafson, Noise improvements in quantum simulations of SQED using qutrits, arXiv:2201.04546.

[23] H. Bechmann-Pasquinucci and A. Peres, Quantum cryptography with 3-state systems, Phys. Rev. Lett. **85**, 3313 (2000).

[24] D. Bruß and C. Macchiavello, Optimal eavesdropping in cryptography with three-dimensional quantum states, Phys. Rev. Lett. **88**, 127901 (2002).

[25] A. Vaziri, G. Weihs, and A. Zeilinger, Experimental two-photon, three-dimensional entanglement for quantum communication, Phys. Rev. Lett. **89**, 240401 (2002).

[26] M. Fitzi, N. Gisin, and U. Maurer, Quantum solution to the byzantine agreement problem, Phys. Rev. Lett. **87**, 217901 (2001).

[27] T. C. Ralph, K. J. Resch, and A. Gilchrist, Efficient toffoli gates using qudits, Phys. Rev. A **75**, 022313 (2007).

[28] M. Fujiwara, M. Takeoka, J. Mizuno, and M. Sasaki, Exceeding the classical capacity limit in a quantum optical channel, Phys. Rev. Lett. **90**, 167906 (2003).

[29] A. C. Y. Li, M. S. Alam, T. Iadecola, A. Jahin, D. M. Kurkcuoglu, R. Li, P. P. Orth, A. B. Özgüler, and G. N. Perdue, Benchmarking variational quantum eigensolvers for the square-octagon-lattice Kitaev model, Phys. Rev. Res. **5**, 033071 (2023).

[30] A. B. Özgüler and D. Venturelli, Numerical gate synthesis for quantum heuristics on bosonic quantum processors, Front. Phys. **10**, 900612 (2022).

[31] C. Cao, J. Xue, N. Shannon, and R. Joynt, Speedup of the quantum adiabatic algorithm using delocalization catalysis, Phys. Rev. Res. **3**, 013092 (2021).

[32] A B. Özgüler, R. Joynt, and M. G. Vavilov, Steering random spin systems to speed up the quantum adiabatic algorithm, Phys. Rev. A **98**, 062311 (2018).

[33] A. B. Özgüler, V. E. Manucharyan, and M. G. Vavilov, Excitation dynamics in inductively coupled fluxonium circuits, arXiv:2104.03300.

[34] A. B. Özgüler, C. Xu, and M. G. Vavilov, Response of a quantum disordered spin system to a local periodic drive, Phys. Rev. B **101**, 024204 (2020).

[35] G. K. Brennen, D. P. O'Leary, and S. S. Bullock, Criteria for exact qudit universality, Phys. Rev. A **71**, 052318 (2005).

[36] A. Muthukrishnan and C. R. Stroud, Multivalued logic gates for quantum computation, Phys. Rev. A **62**, 052309 (2000).

[37] D. L. Zhou, B. Zeng, Z. Xu, and C. P. Sun, Quantum computation based on d-level cluster state, Phys. Rev. A **68**, 062303 (2003).

[38] M. S. Blok, V. V. Ramasesh, T. Schuster, K. O'Brien, J. M. Kreikebaum, D. Dahlen, A. Morvan, B. Yoshida, N. Y. Yao, and I. Siddiqi, Quantum information scrambling on a superconducting qutrit processor, Phys. Rev. X **11**, 021010 (2021).

[39] L. E. Fischer, A. Chiesa, F. Tacchino, D. J. Egger, S. Carretta, and I. Tavernelli, Universal qudit gate synthesis for transmons, PRX Quantum **4**, 030327 (2023).

[40] N. Goss, A. Morvan, B. Marinelli, B. K. Mitchell, L. B. Nguyen, R. K. Naik, L. Chen, C. Jünger, J. M. Kreikebaum, D. I. Santiago, J. J. Wallman, and I. Siddiqi, High-fidelity qutrit entangling gates for superconducting circuits, Nat. Commun. **13**, 7481 (2022).

[41] Y. Chi, J. Huang, Z. Zhang, J. Mao, Z. Zhou, X. Chen, C. Zhai, J. Bao, T. Dai, H. Yuan *et al.*, A programmable qudit-based quantum processor, Nat. Commun. **13**, 1166 (2022).

[42] P. Hrmo, B. Wilhelm, L. Gerster, M. W. van Mourik, M. Huber, R. Blatt, P. Schindler, T. Monz, and M. Ringbauer, Native qudit entanglement in a trapped ion quantum processor, Nat. Commun. **14**, 2242 (2023).

[43] M. Ringbauer, M. Meth, L. Postler, R. Stricker, R. Blatt, P. Schindler, and T. Monz, A universal qudit quantum processor with trapped ions, Nat. Phys. **18**, 1053 (2022).

[44] Y. Atia and D. Aharonov, Fast-forwarding of hamiltonians and exponentially precise measurements, Nat. Commun. **8**, 1572 (2017).

[45] F. Barratt, J. Dborin, M. Bal, V. Stojevic, F. Pollmann, and A. G. Green, Parallel quantum simulation of large systems on small nisq computers, npj Quantum Inf. **7**, 79 (2021).

[46] N. F. Berthusen, T. V. Trevisan, T. Iadecola, and P. P. Orth, Quantum dynamics simulations beyond the coherence time on noisy intermediate-scale quantum hardware by variational trotter compression, Phys. Rev. Res. **4**, 023097 (2022).

[47] D. Camps, E. Kökcü, L. B. Oftelie, W. A. de Jong, A. F. Kemper, and R. Van Beeumen, An algebraic quantum circuit compression algorithm for Hamiltonian simulation, SIAM J. Matrix Anal. Appl. **43**, 1084 (2022).

[48] C. Cîrstoiu, Z. Holmes, J. Iosue, L. Cincio, P. J. Coles, and A. Sornborger, Variational fast forwarding for quantum simulation beyond the coherence time, npj Quantum Inf. **6**, 82 (2020).

[49] E. Kökcü, D. Camps, L. Bassman, J. K. Freericks, W. A. de Jong, R. Van Beeumen, and A. F. Kemper, Algebraic compression of quantum circuits for Hamiltonian evolution, Phys. Rev. A **105**, 032420 (2022).

[50] S.-H. Lin, R. Dilip, A. G. Green, A. Smith, and F. Pollmann, Real-and imaginary-time evolution with compressed quantum circuits, PRX Quantum **2**, 010342 (2021).

[51] L. B. Oftelie, R. Van Beeumen, Ed Younis, E. Smith, C. Iancu, and W. A. de Jong, Constant-depth circuits for dynamic simula-

tions of materials on quantum computers, Mater. Theory **6**, 13 (2022).

[52] C.-N. Yang, Some exact results for the many-body problem in one dimension with repulsive delta-function interaction, Phys. Rev. Lett. **19**, 1312 (1967).

[53] R. J. Baxter, *Exactly Solved Models in Statistical Mechanics* (Elsevier, Amsterdam, 2016).

[54] M. T. Batchelor and A. Foerster, Yang-Baxter integrable models in experiments: from condensed matter to ultracold atoms, J. Phys. A **49**, 173001 (2016).

[55] M.-L. Ge, K. Xue, R.-Y. Zhang, and Q. Zhao, Yang-Baxter equations and quantum entanglements, Quant. Info. Proc. **15**, 5211 (2016).

[56] S. Gulania, Z. He, B. Peng, N. Govind, and Y. Alexeev, QuYBE: An algebraic compiler for quantum circuit compression, in *2022 IEEE/ACM 7th Symposium on Edge Computing (SEC)* (IEEE, New York, 2022), pp. 406–410.

[57] L. H. Kauffman and S. J. Jr. Lomonaco, Topological quantum information theory, in *Proceedings of Symposia in Applied Mathematics*, edited by S. J. Lomonaco (AMS, Washington, DC, 2010), Vol. 68.

[58] C. Nayak, S. H. Simon, A. Stern, M. Freedman, and S. D. Sarma, Non-Abelian anyons and topological quantum computation, Rev. Mod. Phys. **80**, 1083 (2008).

[59] B. Peng, S. Gulania, Y. Alexeev, and N. Govind, Quantum time dynamics employing the Yang-Baxter equation for circuit compression, Phys. Rev. A **106**, 012412 (2022).

[60] F. A. Vind, A. Foerster, I. S. Oliveira, R. S. Sarthour, D. de O. Soares-Pinto, A. M. de Souza, and I. Roditi, Experimental realization of the Yang-Baxter equation via NMR interferometry, Sci. Rep. **6**, 20789 (2016).

[61] Y. Zhang, Integrable quantum computation, Quant. Info. Proc. **12**, 631 (2013).

[62] H. Wang, S. Wei, C. Zheng, X. Kong, J. Wen, X. Nie, J. Li, D. Lu, and T. Xin, Experimental simulation of the four-dimensional Yang-Baxter equation on a spin quantum simulator, Phys. Rev. A **102**, 012610 (2020).

[63] C. Zheng, J. lin Li, S. yu Song, and G. L. Long, Direct experimental simulation of the Yang-Baxter equation, J. Opt. Soc. Am. B **30**, 1688 (2013).

[64] R. S. Chen, Generalized Yang-Baxter equations and braiding quantum gates, J. Knot Theory Ramif. **21**, 1250087 (2012).

[65] C. Galindo, S.-M. Hong, and E. C. Rowell, Generalized and quasi-localizations of braid group representations, Int. Math. Res. Notices **2013**, 693 (2013).

[66] A. P. Isaev, Lectures on quantum groups and Yang-Baxter equations, arXiv:2206.08902.

[67] E. C. Rowell, A quaternionic braid representation (after Goldschmidt and Jones), arXiv:1006.4808.

[68] E. C. Rowell, Y. Zhang, Y.-S. Wu, and M.-L. Ge, Extraspecial two-groups, generalized Yang-Baxter equations and braiding quantum gates, Quantum Inf. Comput. **10**, 685 (2010).

[69] It is interesting to see how to implement these spin-1 operators using spin-1/2 matrices. Taking Eq. (2.7) as an example, we can expand it to a $4 \times 4$ matrix and represent using spin-1/2 Pauli

matrices

$$\tilde{S}^x = \begin{pmatrix} 0 & 0 & 0 \\ 0 & 0 & i \\ 0 & -i & 0 \end{pmatrix} \Rightarrow \begin{pmatrix} 0 & 0 & 0 & 0 \\ 0 & 0 & i & 0 \\ 0 & -i & 0 & 0 \\ 0 & 0 & 0 & 0 \end{pmatrix}$$

$$= I_2 \otimes A - A \otimes I_2 \tag{C4}$$

where $A = \frac{1}{2}(-iX_2 + Y_2)$, and $I_2, X_2,$ and $Y_2$ are spin-1/2 Pauli matrices:

$$I_2 = \begin{pmatrix} 1 & 0 \\ 0 & 1 \end{pmatrix}, X_2 = \begin{pmatrix} 0 & 1 \\ 1 & 0 \end{pmatrix}, Y_2 = \begin{pmatrix} 0 & -i \\ i & 0 \end{pmatrix}. \tag{C5}$$

[70] J. R. Johansson, P. D. Nation, and F. Nori, QuTiP: An open-source python framework for the dynamics of open quantum systems, Comput. Phys. Commun. **183**, 1760 (2012).

[71] J. R. Johansson, P. D. Nation, and F. Nori, QuTiP 2: A Python framework for the dynamics of open quantum systems, Comput. Phys. Commun. **184**, 1234 (2013).

[72] D. Xu, A. B. Özgüler, G. D. Guglielmo, N. Tran, G. N. Perdue, L. Carloni, and F. Fahim, Neural network accelerator for quantum control, in *Proceedings of the 2022 IEEE/ACM Third International Workshop on Quantum Computing Software (QCS), Dallas, TX, USA* (IEEE Computer Society, 2002), pp. 43–49.

[73] M. Krenn, J. Landgraf, T. Foesel, and F. Marquardt, Artificial intelligence and machine learning for quantum technologies, Phys. Rev. A **107**, 010101 (2023).